Available online at www.sciencedirect.com
SCIENCE DIRECT®
Journal of Sound and Vibration 290 (2006) 209–222
JOURNAL OF SOUND AND VIBRATION
www.elsevier.com/locate/jsvi

# Critical speeds and the response of a spinning disk to a stationary load using Mindlin plate theory

Hassan Eid, George G. Adams*

*Mechanical and Industrial Engineering Department, Northeastern University, Boston, MA 02115, USA*

Received 8 March 2004; received in revised form 22 March 2005; accepted 26 March 2005
Available online 16 June 2005

**Abstract**

The critical speeds of a moderately thick circular spinning disk are determined using the Mindlin plate theory, which includes shear deformation and rotational inertia. A combination of analytical and numerical methods is used to calculate the four lowest critical speeds for a centrally clamped uniform circular disk and for different thicknesses and clamping ratios. Comparisons between the critical speeds and the corresponding critical speeds for the classical theory, which neglects shear deformation and rotational inertia, are made. The displacement response at the position of the applied force is also determined for different thickness and clamping ratios and compared with the corresponding results from the classical case.


## 1. Introduction

The literature contains numerous descriptions and applications of various plate theories. In the classical linear thin plate theory, introduced by Kirchhoff (see e.g. Ref. [1]), the effect of transverse shear deformation is neglected. Thus this theory assumes that the normal to the undeformed middle plane remains straight and normal to the deformed middle plane of the plate. Based on these assumptions, the governing differential equation is of fourth order in conjunction with two boundary conditions at each edge. Starting in 1945 with Reissner [2], several investigators have

*Corresponding author. Fax: +1 617 373 2921.
*E-mail address:* adams@coe.neu.edu (G.G. Adams).

0022-460X/$ - see front matter © 2005 Elsevier Ltd. All rights reserved.
doi:10.1016/j.jsv.2005.03.019

**Nomenclature**

| | |
|---|---|
| $a$ | outer radius of the disk |
| $b$ | inner radius of the disk |
| $h$ | thickness of the disk |
| $p$ | Fourier mode number |
| $q_0(r,\theta)$ | external transverse force |
| $r$ | radial coordinate |
| $t$ | time |
| $u_r$ | radial displacement of the disk |
| $u_\theta$ | tangential displacement of the disk |
| $u_z$ | axial displacement of the disk |
| $w$ | transverse deflection of the disk |
| $z$ | axis normal to the plane of the disk |
| $D$ | flexural rigidity $= Eh^3/[12/(1-\nu^2)]$ |
| $E$ | Young's modulus |
| $F$ | Fourier component of the angular rotation of the normal to the middle plane in radial direction |
| $H$ | Fourier component of the angular rotation of the normal to the middle plane in circumferential direction |
| $G$ | modulus of rigidity |
| $M_{rr}$ | radial bending moment per unit length |
| $\bar{M}_{RR}$ | dimensionless radial bending moment per unit length |
| $M_{r\theta}$ | twisting moment per unit length |
| $\bar{M}_{R\theta}$ | dimensionless twisting moment per unit length |
| $M_{\theta\theta}$ | tangential bending moment per unit length |
| $\bar{M}_{\theta\theta}$ | dimensionless tangential bending moment per unit length |
| $Q_r$ | radial shear force per unit length |
| $Q_\theta$ | tangential shear force per unit length |
| $\bar{Q}_0$ | Fourier component of the external transverse force |
| $R$ | dimensionless radial coordinate |
| $T$ | dimensionless time |
| $V$ | Fourier component of the transverse deflection of the middle plane disk |
| $W$ | dimensionless transverse deflection of the disk |
| $\theta$ | angular coordinate (body-fixed) |
| $\kappa^2$ | shear coefficient $= \pi^2/12$ |
| $\nu$ | Poisson's ratio |
| $\rho$ | mass density of the disk |
| $\phi$ | angular coordinate (space-fixed) |
| $\psi_r$, $\psi_\theta$ | angular rotations of the normal to the middle plane in radial and circumferential directions |
| $\omega$ | angular velocity of the disk |
| $\Omega$ | dimensionless angular velocity of the disk |

made improvements to Kirchhoff's theory by including the effect of transverse shear deformation. Because this paper had the most impact upon this subject, the thick plate static theory is usually referred to as Reissner plate theory. The dynamic thick plate theory, which carries Mindlin's name [3], also includes the effect of rotary inertia as it is necessary in dynamics. Mindlin's theory regards the normals to the original middle plane to remain straight but not necessarily normal to the middle plane after deformation, i.e. it allows these lines to rotate with respect to the middle plane. These effects cause the governing differential equation to be of six order and subject to three boundary conditions along each edge.

The determination of the dynamic response of rotating disks, i.e. the mode shapes, natural frequencies and critical speeds, is an important prerequisite to the design of rotating equipment. Classical applications include bladed disk assemblies (for turbines) and flywheels. The earliest study of a vibrating, spinning, elastic disk appears to be that of Lamb and Southwell [4], who derived the linearized equations of transverse deflection and identified the respective contributions to the equations from bending stiffness and in-plane stress due to rotation.

Over the past 20 years, another important use of rotating disks has been in the magnetic and optical storage of data either on hard or flexible disks. Thus many authors have studied spinning

circular and annular plates extensively. Iwan and Moeller [5] used an approximate method in order to estimate the stability characteristics of a rotating disk subject to a concentrated transverse load system. The problem of a stationary nonaxisymmetric load distribution acting on a rotating disk was studied by Benson and Bogy [6]. They found that the membrane operator was singular so that the effect of bending stiffness, no matter how small, still had to be included in the problem formulation. The steady-state response of a flexible thin spinning disk with a transverse load has been studied by Benson [7] near the singular limit of an extremely small ratio of bending to membrane stiffnesses.

Adams [8] studied the effect of a baseplate, as in a magnetic recording application, on the critical speeds of the spinning disk. The presence of the baseplate beneath the disk causes the disk to deform downward toward the baseplate resulting in a stabilizing effect on its transverse motion. In Ref. [8] an elastic foundation is used to approximate the effect of a thin air film separating the spinning disk from the stationary baseplate. Its presence tends to raise the critical speeds of the disk. Benson and Takahashi [9] reviewed the study of the basic mechanical behavior of elastic spinning disks with an emphasis on magnetic storage applications. The resonance and stability issues that affect the magnetic recording interface were identified. The mechanisms that allow the resonance characteristics of the disk to be improved, either by spinning the disk in close proximity to a baseplate or by using a ''stretched surface'' disk, were elucidated. The presence of a recording head can excite resonance, but if properly constructed can enforce a close spacing and high coupling stiffness between the head and the flexible media.

Hosaka and Crandall [10] studied the self-excited vibrations of a flexible disk rotating on an air film above a flat surface without a load system. They solved the coupled disk and air-film equations based on the finite difference technique and compared the results with a single-mode approximation, getting good agreement of the two techniques in calculating the critical speeds. Huang and Mote [11] included two wall enclosure designs. The maximum stable speed for a floppy disk rotating near a rigid surface is shown to be more than 15 times greater than this maximum stable speed without an air film. Renshaw [12] used Lyapunov's method of nonlinear dynamic stability to determine the critical speed of a flexible spinning disk enclosed in a housing that hydrodynamically couples the transverse motion of the disk to the motion of the thin air films surrounding the disk. The hydrodynamically coupled critical speed is three to ten times higher than the uncoupled critical speed, depending on the clamping ratio.

Lee et al. [13] experimentally studied the dynamic response, critical speeds and aerodynamic flutter instability of various optical disks. An experimental estimation technique for the flutter speed of a hard disk based on the measurements taken at subcritical speed, is presented by Hansen et al. [14]. An experimental method for predicting flutter of a spinning disk in a fluid medium, based on the rotating damping model where the relationship between the speed of the disk and the damping force is obtained experimentally, is proposed by Kim et al. [15].

Chen and Bogy [16,17] investigated the stability of a flexible disk drive by including the effects of pitching parameters and frictions forces in the load system. Phylactopoulos and Adams [18] investigated the free vibration of a rectangularly orthotropic annular spinning disk. The forced response of a rectangularly orthotropic spinning disk to a point-load, including the determination of critical speeds is found by Phylactopoulos and Adams [19]. Liang et al. [20] studied vibration and stability of a spinning polar orthotropic disk with a concentrated transverse load modeled as a mass–spring–dashpot system.

Lacey and Talke [21] studied the effect of transverse shear deformation on the spacing in the tape-to-head interface of a longitudinal magnetic recording tape device. The effect of shear deformation would, at first, appear to be negligible because the ratio of tape thickness (28 μm) to tape span (10 μm) is extremely small. However, the magnetic head is 0.35 mm in length and it is a self-acting air bearing with a complex pressure distribution within a small portion (100 μm) of the recording head which produces the tape deflection. Thus the ratio of tape thickness to this characteristic length becomes a significant factor in predicting the head-to-tape spacing [21]. The effect of shear deformation was important in this crucial region of the head-to-tape interface. Without shear deformation the maximum spacing in the central 50 μm region was about 95 μm whereas with shear deformation it was approximately 75 μm. It may appear counterintuitive that this displacement is less with shear deformation than it is without. Note, however, that in this nonlinear problem the air bearing force, with shear deformation, is decreased because the additional compliance allows the tape to conform more closely to the head profile.

In this paper, the critical speeds and the response of a spinning disk to a stationary load are studied using the assumptions of the Mindlin theory of thick plates, which includes the effects of transverse shear deformation and rotary inertia. Comparisons are made with available solutions which use the classical plate theory [8]. In addition to being of general theoretical interest, the effects of shear deformation and rotational inertia may be important in magnetic recording applications on flexible disks. As in magnetic tape devices, the characteristic length is a small fraction of the recording head length. Thus although the disk thickness may be an extremely small fraction of the disk radius, it may be a reasonable fraction of this characteristic length associated with a portion of the recording head.

## 2. Mathematical model formulation

The dynamical governing equations of motion of the spinning Mindlin circular disk are obtained [3,22, and 23] in terms of the stress resultants, by applying Newton's second law to a differential element as shown in Fig. 1

$$\frac{\partial M_{rr}}{\partial r}+\frac{1}{r}\frac{\partial M_{r\theta}}{\partial \theta}+\frac{M_{rr}-M_{\theta\theta}}{r}-Q_r=\frac{\rho h^3}{12}\frac{\partial^2 \psi_r}{\partial t^2}, \tag{1a}$$

$$\frac{\partial M_{r\theta}}{\partial r}+\frac{1}{r}\frac{\partial M_{\theta\theta}}{\partial \theta}+\frac{2}{r}M_{r\theta}-Q_\theta=\frac{\rho h^3}{12}\frac{\partial^2 \psi_\theta}{\partial t^2}, \tag{1b}$$

$$\frac{\partial Q_r}{\partial r}+\frac{1}{r}\frac{\partial Q_\theta}{\partial \theta}+\frac{Q_r}{r}+\frac{h}{r}\frac{\partial}{\partial r}\left(r\sigma_{rr}\frac{\partial w}{\partial r}\right)+\frac{h}{r^2}\sigma_{\theta\theta}\frac{\partial^2 w}{\partial \theta^2}+q_0(r,\theta,t)=\rho h\frac{\partial^2 w}{\partial t^2}, \tag{1c}$$

where the displacement field components in Mindlin's theory of plates are assumed to have the forms

$$u_r=z\psi_r(r,\theta,t),\quad u_\theta=z\psi_\theta(r,\theta,t),\quad u_z=w(r,\theta,t)\,. \tag{2}$$

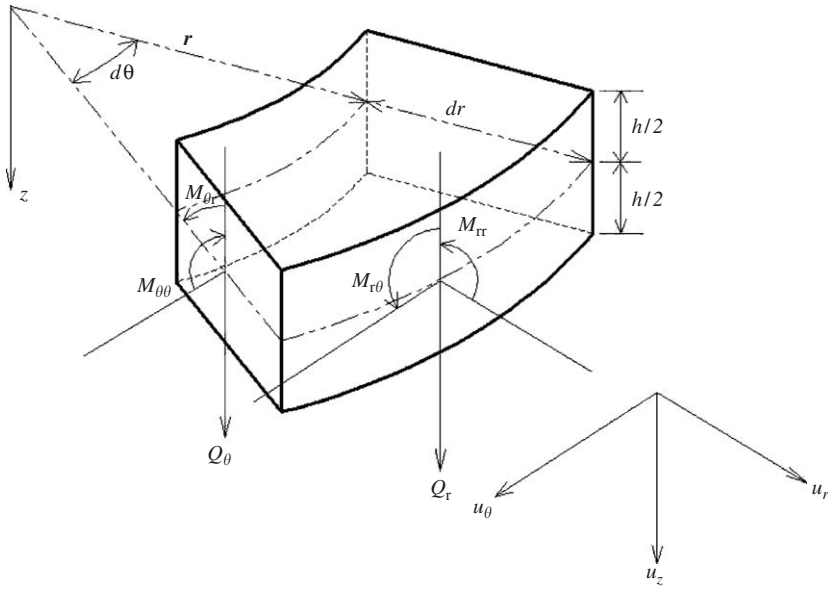


Fig. 1. Displacements and stress resultants on a differential element of a circular disk in cylindrical coordinates.

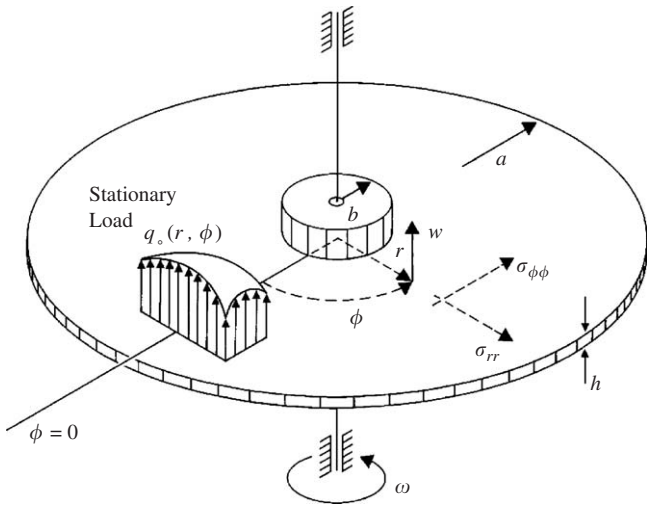


Fig. 2. Rotating flexible disk acted upon by a stationary load distribution.

The quantities $\psi_r$ and $\psi_\theta$ correspond to the angles of rotations of the normal to the cross-section (in the $rz$-plane and in the $\theta z$-plane, respectively) which produce radial and tangential displacements respectively through the plate thickness.

The faces of the disk are taken to be free from tangential traction but are under normal pressure $q_0(r, \theta, t)$ which, in a magnetic recording application, acts in the air bearing between the disk and the read–write head (Fig. 2). In Eqs. (1), the corresponding bending moments per unit length ($M_{rr}, M_{\theta\theta}, M_{r\theta}$) and shear forces ($Q_r, Q_\theta$) per unit length in a linearly elastic and isotropic circular

Mindlin disk can be written in terms of the lateral deflection $w$ and angular rotations $\psi_r, \psi_\theta$ using the stress–strain laws for plane stress as

$$M_{rr} = D\left[\frac{\partial \psi_r}{\partial r} + \frac{v}{r}\left(\psi_r + \frac{\partial \psi_\theta}{\partial \theta}\right)\right], \tag{3}$$

$$M_{\theta\theta} = D\left[\frac{1}{r}\left(\psi_r + \frac{\partial \psi_\theta}{\partial \theta}\right) + v\frac{\partial \psi_r}{\partial r}\right], \tag{4}$$

$$M_{r\theta} = D\frac{(1-v)}{2}\left[\frac{1}{r}\left(\frac{\partial \psi_r}{\partial \theta} - \psi_\theta\right) + \frac{\partial \psi_\theta}{\partial r}\right], \tag{5}$$

$$Q_r = \kappa^2 Gh\left(\psi_r + \frac{\partial w}{\partial r}\right), \tag{6}$$

$$Q_\theta = \kappa^2 Gh\left(\psi_\theta + \frac{1}{r}\frac{\partial w}{\partial \theta}\right). \tag{7}$$

In Eqs. (1)–(7) $h$ and $E$ are the uniform disk thickness and Young's modulus, respectively, and $D = Eh^3/[12(1-v^2)]$ is the bending rigidity. Furthermore, $w(r,\theta,t)$ is the transverse displacement of the middle plane of the disk at the polar location $(r,\theta)$ and at time $t$. Finally, $v$ and $\rho$ are the Poisson's ratio and mass density of the disk, respectively and the value of $\pi^2/12$ is used for the shear correction factor $\kappa^2$ [22].

Corresponding to a spinning disk clamped at its inner radius ($r = b$) and free at its outer radius ($r = a$), the expressions for in-plane centrifugal membrane radial and tangential stresses are denoted by $\sigma_{rr}$ and $\sigma_{\theta\theta}$ in Eqs. (1). These stresses are proportional to the square of the disk angular velocity $\omega$, are independent of $\theta$, and can be found by integrating the displacement form of the radial equation of motion for the spinning disk. The stresses $\sigma_{rr}$ and $\sigma_{\theta\theta}$ are given by [8]

$$\sigma_{rr}(r) = \frac{\rho\omega^2}{8}(3+v)(a^2 - r^2)\left[1 + \frac{1-v}{3+v}\gamma b^2/r^2\right], \tag{8a}$$

$$\sigma_{\theta\theta}(r) = \frac{\rho\omega^2}{8}\left[(1+v)(b^2 + \gamma a^2) - (1+3v)r^2 - (1-v)\gamma b^2 a^2/r^2\right], \tag{8b}$$

where the dimensionless parameter $\gamma$ is defined as

$$\gamma = [(3+v)a^2 - (1+v)b^2]/[(1+v)a^2 + (1-v)b^2].$$

The following dimensionless quantities are now introduced:

$$R = r/a, \quad W = w/a, \quad \Psi_R = \psi_r, \quad \Psi_\theta = \psi_\theta,$$

$$Q_0 = q_0/G, \quad \bar{M}_R = M_r/(D/a), \quad \bar{M}_\theta = M_\theta/(D/a), \quad \bar{M}_{R\theta} = M_{r\theta}/(D/a), \tag{9}$$

$$T = \frac{t}{a}\sqrt{E/[\rho(1-v^2)]}, \quad \Omega = a\omega\sqrt{\rho(1-v^2)/E}.$$

The dynamical equations of motion of a circular disk in dimensionless form are then transformed from a body-fixed frame of reference $(R, \theta, T)$ to a space-fixed reference frame $(R, \phi, T)$, by using a Galilean transformation. The angular coordinates of the two reference frames are related to each other by

$$\phi = \theta + \omega t = \theta + \Omega T. \tag{10}$$

Assuming that the derivatives of $\psi_r, \psi_\theta$ and $W$ with respect to $T$ are zero in the space-fixed reference frame $(R, \phi)$, leads to the steady-state solution. By using the non-dimensional quantities in the space-fixed frame (9), Eqs. (3) can be rewritten as

$$R^2\frac{\partial^2\tilde{\Psi}_R}{\partial R^2} + R\frac{\partial\tilde{\Psi}_R}{\partial R} - (1+\eta R^2)\tilde{\Psi}_R + \frac{(1-\nu)}{2}\frac{\partial^2\tilde{\Psi}_R}{\partial\phi^2} + \frac{(1+\nu)}{2}R\frac{\partial^2\tilde{\Psi}_\theta}{\partial R\partial\phi} - \frac{(3-\nu)}{2}\frac{\partial\tilde{\Psi}_\phi}{\partial\phi} - \eta R^2\frac{\partial\tilde{W}}{\partial R} = R^2\Omega^2\frac{\partial^2\tilde{\Psi}_R}{\partial\phi^2}, \tag{11a}$$

$$\frac{(1+\nu)}{2}R\frac{\partial^2\tilde{\Psi}_R}{\partial\phi\partial R} + \frac{(3-\nu)}{2}\frac{\partial\tilde{\Psi}_R}{\partial\phi} + \frac{\partial^2\tilde{\Psi}_\phi}{\partial\phi^2} + \frac{(1-\nu)}{2}R^2\frac{\partial^2\tilde{\Psi}_\phi}{\partial R^2} + \frac{(1-\nu)}{2}R\frac{\partial\tilde{\Psi}_\phi}{\partial R} - \left(\frac{(1-\nu)}{2} + \eta R^2\right)\tilde{\Psi}_\phi - \eta R\frac{\partial\tilde{W}}{\partial\phi} = R^2\Omega^2\frac{\partial^2\tilde{\Psi}_\phi}{\partial\phi^2}, \tag{11b}$$

$$R^2\frac{\partial\tilde{\Psi}_R}{\partial R} + \eta R^2\frac{\partial^2\tilde{W}}{\partial R^2} + R\frac{\partial\tilde{\Psi}_\phi}{\partial\phi} + \frac{\partial^2\tilde{W}}{\partial\phi^2} + R\tilde{\Psi}_R + R\frac{\partial\tilde{W}}{\partial R} + \left(\frac{1}{\kappa^2 G}\right)\left\{R\frac{\partial}{\partial R}\left(R\sigma_{RR}\frac{\partial\tilde{W}}{\partial R}\right) + \sigma_{\phi\phi}\frac{\partial^2\tilde{W}}{\partial\phi^2}\right\} + \left(\frac{a}{\kappa^2 h}\right)R^2\tilde{Q}_0 = \frac{2R^2}{\kappa^2(1-\nu)}\frac{\partial^2\tilde{W}}{\partial\phi^2}, \tag{11c}$$

where $\eta = 6\kappa^2 a^2(1-\nu)/h^2$.

To avoid the singularity in Mindlin disk theory due to the shear deformation effect when the external normal force $q_0(r, \theta)$ is a concentrated point load, it is convenient to express the external load using the Heaviside step function $H(\bullet)$ in the $(r, \phi)$ directions. The load is assumed to act over a finite area of radial length $\Delta r$ and angular extent $\Delta\phi$, with center at the position $(R_0, 0)$. The dimensionless form of $\tilde{Q}_0(R, \phi)$ in the fixed-frame reference is mathematically expressed as

$$\tilde{Q}_0(R,\phi) = \frac{1}{R_0\,\Delta R\,\Delta\varphi}\left[H\left(\frac{\Delta R}{2} - |R - R_0|\right)H\left(\frac{\Delta\varphi}{2} - \phi\right)\right], \tag{12}$$

i.e. it is a uniform load in a sector-shaped region.

In order to eliminate the angular coordinate, we expand the transverse deflection, angular rotations of the normal to the middle plane, and the external force as exponential Fourier series using

$$\tilde{W}(R,\phi) = \sum_{p=-\infty}^{\infty} V_p(R)\mathrm{e}^{\mathrm{i}p\phi}, \qquad V_p(R) = \frac{1}{2\pi}\int_{-\pi}^{\pi}\tilde{W}(R,\phi)\mathrm{e}^{-\mathrm{i}p\phi}\,\mathrm{d}\phi, \tag{13a}$$

$$\tilde{\Psi}_R(R,\phi)=\sum_{p=-\infty}^{\infty}F_p(R)\mathrm{e}^{\mathrm{i}p\phi},\qquad F_p(R)=\frac{1}{2\pi}\int_{-\pi}^{\pi}\tilde{\Psi}_R(R,\phi)\mathrm{e}^{-\mathrm{i}p\phi}\,\mathrm{d}\phi, \tag{13b}$$

$$\tilde{\Psi}_\phi(R,\phi)=\sum_{p=-\infty}^{\infty}H_p(R)\mathrm{e}^{\mathrm{i}p\phi},\qquad H_p(R)=\frac{1}{2\pi}\int_{-\pi}^{\pi}\tilde{\Psi}_\phi(R,\phi)\mathrm{e}^{-\mathrm{i}p\phi}\,\mathrm{d}\phi, \tag{13c}$$

$$\tilde{Q}_0(R,\phi)=\sum_{p=-\infty}^{\infty}\bar{Q}_0(R)\mathrm{e}^{\mathrm{i}p\phi},\qquad \bar{Q}_0(R)=\frac{1}{2\pi}\int_{-\pi}^{\pi}\tilde{Q}_0(R,\phi)\mathrm{e}^{-\mathrm{i}p\phi}\,\mathrm{d}\phi. \tag{13d}$$

This procedure leads to three infinite sets of second-order ordinary differential equations for the Fourier components of the deflection and the angular rotations, i.e.

$$R^2\frac{\mathrm{d}^2F_p}{\mathrm{d}R^2}+R\frac{\mathrm{d}F_p}{\mathrm{d}R}-(1+\eta R^2)F_p-\frac{(1-\nu)}{2}F_p+\frac{(\mathrm{i}p)(1+\nu)}{2}R\frac{\mathrm{d}H_p}{\mathrm{d}R}$$
$$-\frac{(\mathrm{i}p)(3-\nu)}{2}H_p-\eta R^2\frac{\mathrm{d}V_p}{\mathrm{d}R}=-p^2R^2\Omega^2F_p,\quad p=-\infty\text{ to }\infty, \tag{14a}$$

$$\frac{(\mathrm{i}p)(1+\nu)}{2}R\frac{\mathrm{d}F_p}{\mathrm{d}R}+\frac{(\mathrm{i}p)(3-\nu)}{2}F_p-p^2H_p+\frac{(1-\nu)}{2}R^2\frac{\mathrm{d}^2H_p}{\mathrm{d}R^2}$$
$$+\frac{(1-\nu)}{2}R\frac{\mathrm{d}H_p}{\mathrm{d}R}-\left(\frac{(1-\nu)}{2}+\eta R^2\right)H_p-(\mathrm{i}p)\eta RV_p=-p^2R^2\Omega^2H_p,\quad p=-\infty\text{ to }\infty, \tag{14b}$$

$$\left(R^2+s_2\right)R^2\frac{\mathrm{d}^2V_p}{\mathrm{d}R^2}+(R+s_1+s_3+s_4)\frac{\mathrm{d}V_p}{\mathrm{d}R}-\left(p^2+s_5\right)V_p+R^2\frac{\mathrm{d}F_p}{\mathrm{d}R}+RF_p$$
$$+(\mathrm{i}p)RH_p+\left(\frac{a}{\kappa^2h}\right)R^2\bar{Q}_0=\frac{-2p^2R^2\Omega^2}{\kappa^2(1-\nu)}V_p,\quad p=-\infty\text{ to }\infty, \tag{14c}$$

where $s_{1,2,3,4,5}$ represent the membrane stiffness effect of the centrifugal stresses $\sigma_{RR},\sigma_{\phi\phi}$

$$s_1=\frac{\Omega^2R}{4\kappa^2(1-\nu)}(3+\nu)(1-R^2)\left[1+\frac{(1-\nu)}{(3+\nu)}\left(\frac{\gamma}{R^2}\right)\left(\frac{b}{a}\right)^2\right], \tag{15a}$$

$$s_2=\frac{\Omega^2R^2}{4\kappa^2(1-\nu)}(3+\nu)(1-R^2)\left[1+\frac{(1-\nu)}{(3+\nu)}\left(\frac{\gamma}{R^2}\right)\left(\frac{b}{a}\right)^2\right], \tag{15b}$$

$$s_3=\frac{-\Omega^2R^3}{2\kappa^2(1-\nu)}(3+\nu)\left[1+\frac{(1-\nu)}{(3+\nu)}\left(\frac{\gamma}{R^2}\right)\left(\frac{b}{a}\right)^2\right], \tag{15c}$$

$$s_4=\frac{\Omega^2R^2}{4\kappa^2(1-\nu)}(3+\nu)(1-R^2)\left[1-\frac{(1-\nu)}{(3+\nu)}\left(\frac{2\gamma}{R^3}\right)\left(\frac{b}{a}\right)^2\right], \tag{15d}$$

$$s_5 = \frac{-\Omega^2 p^2}{4\kappa^2(1-\nu)}\left[(1+\nu)\left(\left(\frac{b}{a}\right)^2+\gamma\right)-(1+3\nu)R^2-(1-\nu)\left(\frac{\gamma}{R^2}\right)\left(\frac{b}{a}\right)^2\right]. \tag{15e}$$

From Eq. (12) the Fourier component $\bar{Q}_0$ of the external force can be written as

$$\overline{Q_0}(R) = \frac{1}{2\pi R_0 \Delta R} H\left(\frac{\Delta R}{2} - |R - R_0|\right). \tag{16}$$

In the case in which the disk is free at the outside radius, the radial moment, twisting moment, and radial shear each vanish, i.e.

$$M_r = M_{r\theta} = Q_r = 0 \quad \text{at } r = a. \tag{17}$$

When the disk is clamped at the inside radius, the angular rotations of the normal to the middle plane and transverse deflection of the disk are zero, i.e.

$$\psi_r = \psi_\theta = w = 0 \quad \text{at } r = b. \tag{18}$$

The boundary conditions can be rewritten by eliminating the angular coordinate using the exponential Fourier series forms (13) in dimensionless forms related to the fixed-frame reference $(R, \phi)$ as

$$\frac{\mathrm{d}F_p}{\mathrm{d}R} + \nu[F_p + (\mathrm{i}p)H_p] = 0, \quad (\mathrm{i}p)F_p - H_p + \frac{\mathrm{d}H_p}{\mathrm{d}R} = 0, \quad F_p + \frac{\mathrm{d}V_p}{\mathrm{d}R} = 0 \quad \text{at } R = 1, \tag{19a}$$

$$F_p = 0, \quad H_p = 0, \quad V_p = 0, \quad \text{at } R = b/a, \tag{19b}$$

where $p = -\infty$ to $\infty$.

The infinite sets of second-order ordinary differential equations (14) can now be solved using the standard finite difference scheme [24], subject to boundary conditions obtained from Eq. (19a, b) with Eq. (13a–c). The disk deflection at any point is given by

$$W(R, \phi) = V_0(R) + 2\sum_{p=1}^{\infty} V_p(R)\cos(p\phi) \tag{20}$$

in which the symmetric loading has been used to simplify the solution. The method just outlined gives us a procedure for determining the disk deflection for an arbitrary prescribed pressure.

## 3. Numerical applications and discussions

For the sake of numerical comparison, the case of a disk modeled using the classical linear thin plate theory is adopted from Ref. [8]. By applying finite difference approximations to the differential equations (14a–c) with vanishing external transverse force, along with the boundary conditions (19a–b), three sets of linear homogenous algebraic equations results for each value of $p$, which has nontrivial solutions only for certain values of the dimensionless angular velocity ($\Omega$). Thus the vanishing of the determinant determines the critical speeds ($\Omega_c$) at which the spinning disk is unable to support arbitrary spatially stationary load distributions. Each calculation was

done using 100 grid points, although these results differed from those obtained with 200 grid points by less than 0.6%.

It is noted that each normal mode of vibration, when viewed in a reference frame rotating with the disk, can be considered as the sum of two oppositely traveling waves of equal wavelength and amplitude. At a critical speed, the speed of the back-traveling wave is equal to the rotational speed of the disk and is therefore stationary in space. Hence a stationary load causes an unbounded response of the disk.

Figs. 3(a)–(d) display the influence of rotary inertia and transverse shear deformation on the dimensionless lowest critical speed ($\Omega_c$) for each Fourier mode, for a range of clamping radius ratios ($b/a$), and for different thickness to outer radius ratios ($h/a = 0.05, 0.1, 0.2$) as well as for the classical linear thin plate theory. In each instance the lowest critical speed corresponds to zero nodal circles which is similar to what was found in other investigations [9]. From these plots, it becomes apparent that with an increase of the clamping radius ratio, each of the critical speeds at first decreases slightly before eventually increasing. This initial decrease may appear to be

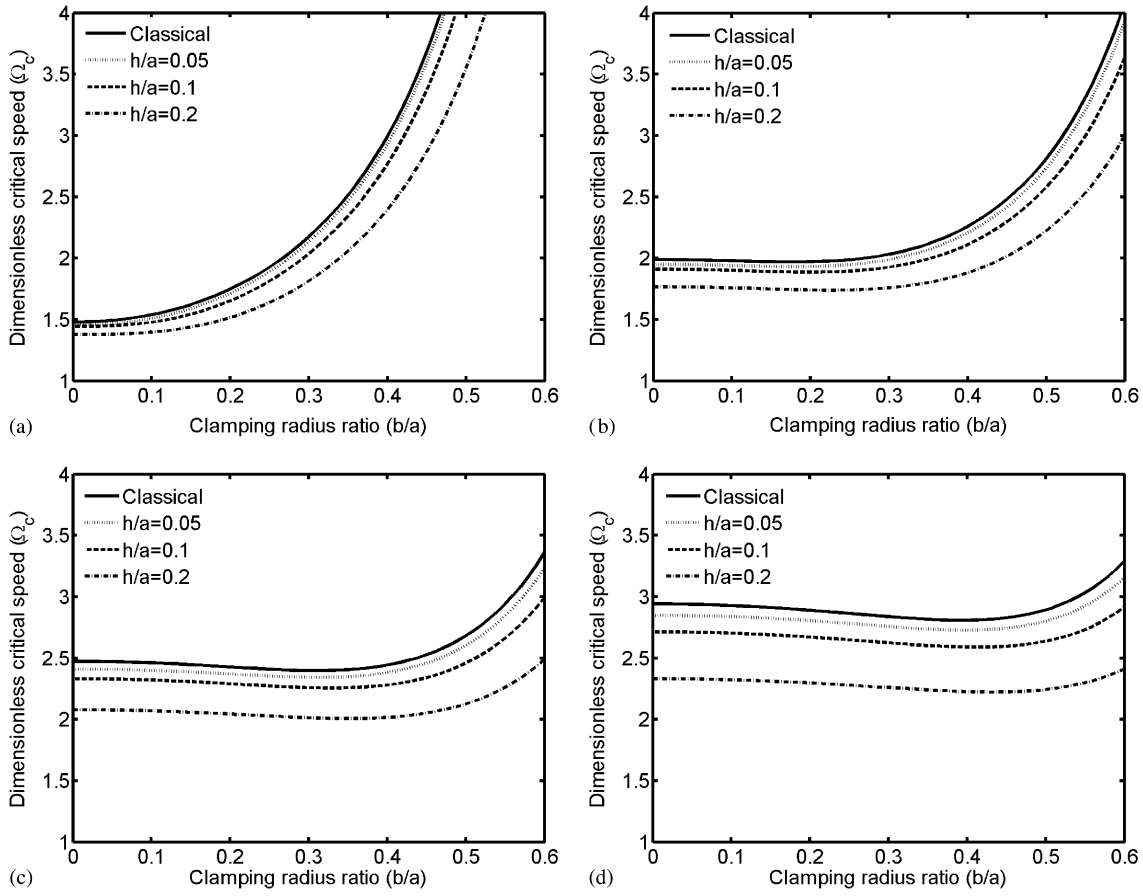


Fig. 3. Dimensionless critical speed ($\Omega_c$) vs. clamping radius ratio ($b/a$) for various thickness ratios ($h/a$): (a) for mode $p = 2$; (b) for mode $p = 3$; (c) for mode $p = 4$; (d) for mode $p = 5$.

counter-intuitive because the bending stiffness of the disk increases monotonically with the clamping ratio ($b/a$) for both the classical and Mindlin disk models. However, the *membrane stress* decreases monotonically with ($b/a$) and it is this effect which causes the initial decline of the lowest critical speed. The results presented in these figures show that, at a small thickness to outer radius ratio ($h/a = 0.05$), the critical speed for the Mindlin disk model approaches the classical disk model. The difference varies from about 2% up to around 4%. The greater deviation is due to the increased effect of transverse shear deformation for higher modes and/or for increased clamping radius ratios.

It is also noted that there are no critical speeds for the first and the zero modes which is similar to previous investigations [9]. It is noted that the Fourier mode number $p$ corresponds to the

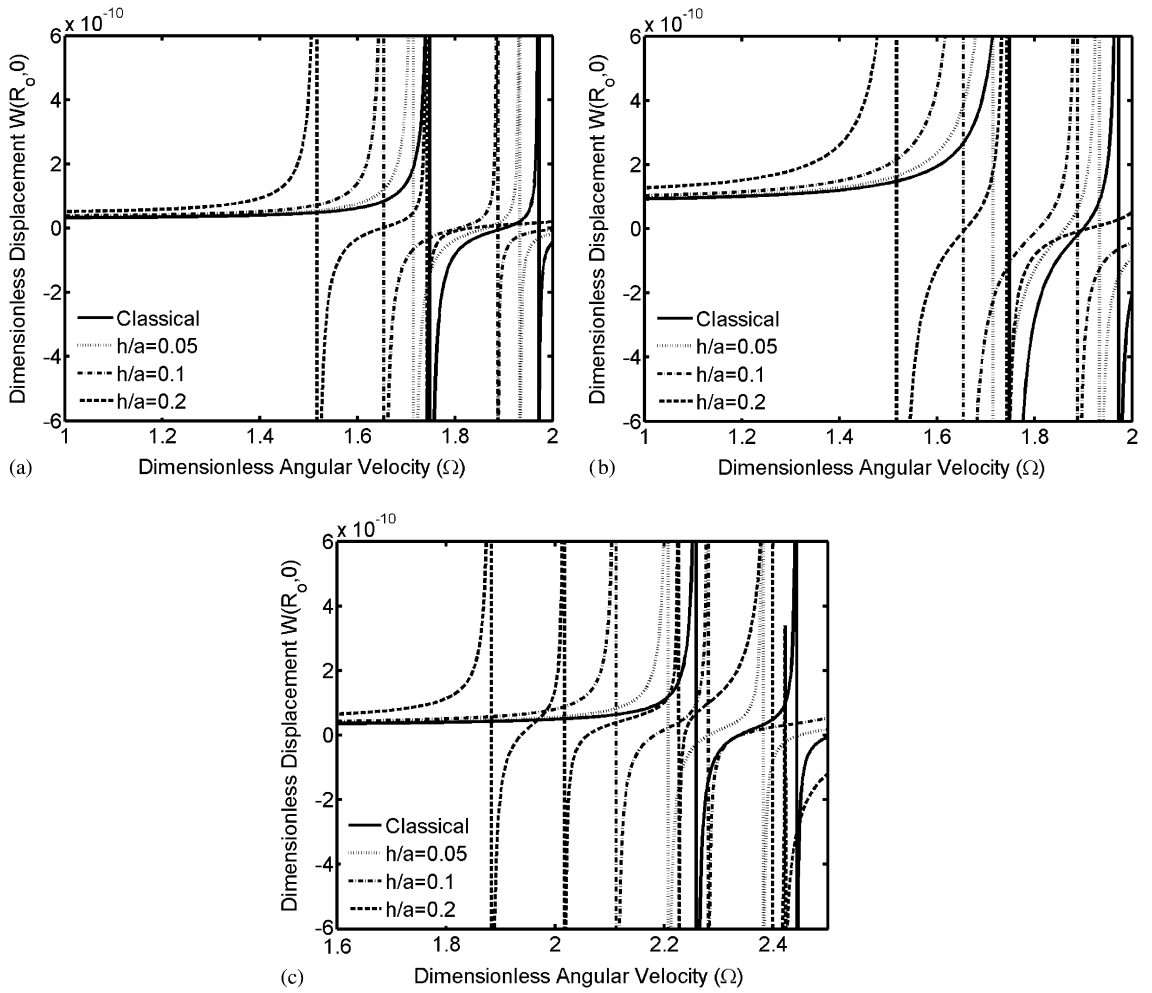


Fig. 4. Dimensionless displacement $W(R_0, 0)$ vs. dimensionless angular velocity ($\Omega$) for various thickness ratios ($h/a$): (a) the location at $R = 0.6$ and clamping ratio $b/a = 0.2$; (b) the load location at $R = 0.8$ and clamping ratio $b/a = 0.2$; (c) the load location at $R = 0.8$ and clamping ratio $b/a = 0.4$.

number of spatial nodal diameters. Thus $p = 0$ is an axisymmetric deformation whereas $p = 1$ would correspond to a rigid body tilt if $b = 0$. The $p = 0$ critical speed would not be expected to exist because the corresponding deflection pattern would increase the strain energy of the system without affecting the kinetic energy. The nonexistence of a critical speed for $p = 1$ was proven analytically by Renshaw and Mote [25] for the classical disk. Such a proof for the Mindlin disk is beyond the scope of this work. The reason for the lack of a $p = 1$ critical speed is that the effect of disk rotation is to stiffen the disk with increasing speed such that the speed of the back-traveling wave is always greater than the rotational speed. Without disk rotation, as in the stationary disk subjected to a moving load system [26], a $p = 1$ critical speed does exist.

In Figs. 4(a)–(c) the displacement at the point of application of the stationary load and its dependence upon the disk spin rate are shown for different thicknesses. The stationary load has been taken over a finite area, with $\Delta R$ equal to the grid spacing in the finite difference scheme and $\Delta\varphi = 0.01$. These results have been calculated with 20 modes and also with 40 modes; when plotted the results were indistinguishable. Each of Figs. 4(a)–(c) is for a different combination of clamping ratio and location of the point load. The influence of the shear deformation and rotary inertia on the displacements is presented for different thickness to outer radius ratios ($h/a = 0.05$, 0.1 and 0.2). Results are for the model case with shear deformation and rotary inertia included and are compared with the corresponding classical model. The effect of increasing the disk spin rate is most pronounced near each critical speed. As the speed increases from just below to just above the critical speed, the displacement undergoes a 180° phase shift with respect to the force. This phenomenon is typical of critical speeds, e.g. Ref. [9]. Also note that as the load moves further to the free edge of the disk and/or the clamping radius ratio decreases, the effect of shear deformation and rotational inertia become greater and the displacement peak becomes broader.

Fig. 5(a), (b) displays the variation of the displacement (at the point of application of the load) with position of the load. An increase of the displacement occurs with the Mindlin theory, with that increase becoming greater when the load location moves toward the free end. This behavior is

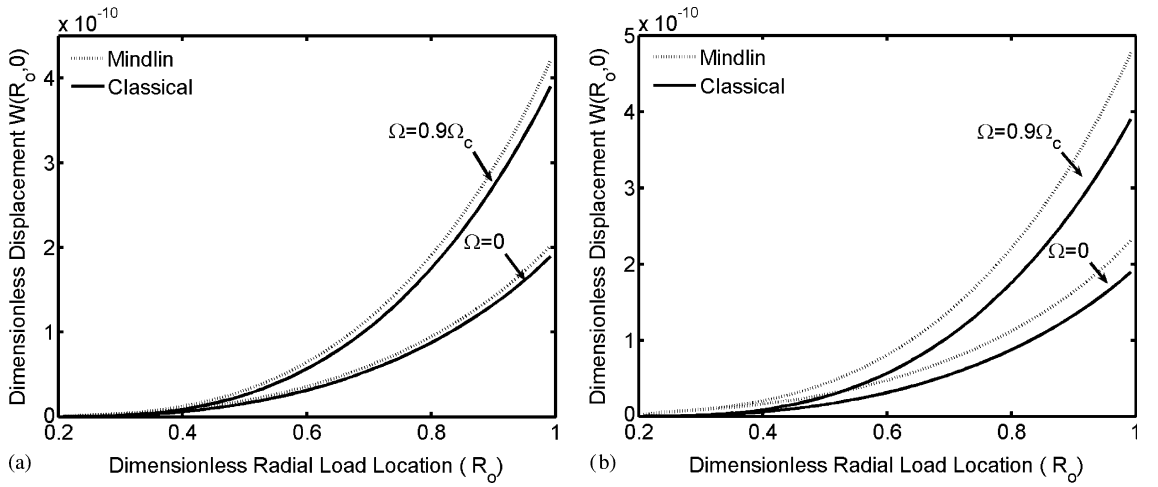


Fig. 5. Dimensionless displacement $W(R_0, 0)$ vs. dimensionless radial load location ($R_0$) for the two theories for two dimensionless angular velocities ($\Omega$): (a) with $b/a = 0.2$ and $h/a = 0.1$; (b) with $b/a = 0.2$ and $h/a = 0.2$.

expected due to the decrease in the disk stiffness toward the free end. The increased displacement is also more prominent for the thicker disk ($h/a = 0.2$) than for the thinner one ($h/a = 0.1$). In these figures, comparisons are made with the corresponding classical model at different speeds ($\Omega = 0$ and $\Omega = 0.9\Omega_c$). The deviation is greatest as the speed increases toward the critical speed.

## 4. Closure

Mindlin's plate theory has been applied to the deformation of a spinning circular disk, centrally clamped and subject to a stationary load. Thus the analysis includes the effects of transverse shear deformation and rotational inertia, which are neglected in the classical plate theory. The results for the Mindlin disk approach those of the classical disk model [8] when the thickness of the disk becomes very small compared to the disk radius. For the thick disk model the results demonstrate a decrease in the critical speeds and an increase in the transverse deflection of the disk. These results are expected due to the influence of shear deformation, especially at greater thickness, larger clamping radius ratios, and for higher modes. This model is of general theoretical interest. In addition it may have relevance in magnetic recording applications even in situations where the disk thickness is a very small fraction of the radius. This is because the characteristic length is dictated by the geometry of the recording head rather than by the disk radius. A similar situation was encountered in magnetic tape applications [21].

## References

[1] S. Timoshenko, S. Woinowsky-Krieger, *Theory of Plates and Shells*, second ed, McGraw-Hill, New York, 1959.
[2] E. Reissner, The effect of transverse shear deformation on the bending of elastic plates, *Journal of Applied Mechanics* 12 (1945) A69–A77.
[3] R.D. Mindlin, Influence of rotary inertia and shear on flexural motions of isotropic, elastic plates, *Journal of Applied Mechanics* 18 (1951) 31–38.
[4] H. Lamb, R.V. Southwell, The vibrations of a spinning disk, *Proceedings of Royal Society, London* 99 (1921) 272–280.
[5] W.D. Iwan, T.L. Moeller, The stability of a spinning elastic disk with a transverse load system, *Journal of Applied Mechanics* 43 (1976) 485–490.
[6] R.C. Benson, D.B. Bogy, Deflection of a very flexible spinning disk due to a stationary transverse load, *Journal of Applied Mechanics* 45 (1978) 636–642.
[7] R.C. Benson, Observations on the steady-state solution of an extremely flexible spinning disk with a transverse load, *Journal of Applied Mechanics* 50 (1983) 525–530.
[8] G.G. Adams, Critical speeds for a flexible spinning disk, *International Journal of Mechanical Science* 27 (1987) 525–531.
[9] R.C. Benson, T.T. Takahashi, Mechanics of flexible disks in magnetic recording, *Advances in Information Storage Systems* 1 (1991) 15–35.
[10] H. Hosaka, S.H. Crandall, Self-excited vibrations of a flexible disk rotating on an air-film above a flat surface, *Acta Mechanica* (Suppl.) 3 (1992) 115–127.
[11] F.Y. Huang, C.D. Mote Jr, On the instability mechanisms of a disk rotating close to a rigid surface, *Journal of Applied Mechanics* 62 (1995) 764–771.
[12] A.A. Renshaw, Critical speed for floppy disks, *Journal of Applied Mechanics* 65 (1998) 116–120.

[13] S.-Y. Lee, J.-D. Kim, S. Kim, Critical and flutter speed of optical disks, *Microsystem Technologies* 8 (2002) 206–211.
[14] M.H. Hansen, A. Raman, C.D. Mote Jr, Estimation of neoconservative aerodynamic pressure leading to flutter of spinning disks, *Journal of Fluids and Structures* 15 (2001) 39–57.
[15] B.C. Kim, A. Raman, C.D. Mote Jr, Prediction of aeroelastic flutter in a hard disk drive, *Journal of Sound and Vibration* 238 (2000) 309–325.
[16] J. Chen, D.B. Bogy, Natural frequencies and stability of flexible spinning disk-stationary load system with rigid body tilting, *Journal of Applied Mechanics* 60 (1993) 470–477.
[17] J. Chen, D.B. Bogy, The effects of a space-fixed friction force on the in-plane stress and stability of transverse vibrations of spinning disk, *Journal of Applied Mechanics* 60 (1993) 646–648.
[18] A. Phylactopoulos, G.G. Adams, Transverse vibration of rectangularly orthotropic spinning disk—part 1: formulation and free vibration, *Journal of Vibration and Acoustics* 121 (1999) 273–279.
[19] A. Phylactopoulos, G.G. Adams, Transverse vibration of rectangularly orthotropic spinning disk—part 2: vibration and critical speeds, *Journal of Vibration and Acoustics* 121 (1999) 280–285.
[20] D.-S. Liang, H.-J. Wang, L.-W. Chen, Vibration and stability of rotating polar orthotropic annular disks subjected to a stationary concentrated transverse load, *Journal of Sound and Vibration* 250 (2002) 795–811.
[21] C. Lacey, F.E. Talke, The effect of head wear and tape shear on the head/tape interface, *Tribology Transactions* 36 (1993) 387–392.
[22] R.D. Mindlin, H. Deresiewicz, Thickness-shear and flexural vibrations of a circular disk, *Journal of Applied Physics* 25 (1954) 1329–1332.
[23] S.K. Sinha, Determination of natural frequencies of a thick spinning annular disk using a numerical Rayleigh–Ritz's trial functions, *Journal of the Acoustical Society of America* 81 (1987) 357–369.
[24] L. Fox, *The Numerical Solution of Two-Point Boundary Problems in Ordinary Differential Equations*, Oxford University Press, London, 1957.
[25] A.A. Renshaw, C.D. Mote Jr, Absence of one nodel diameter critical speed modes in an axisymmetric rotating disk, *Journal of Applied Mechanics* 59 (1992) 687–688.
[26] W.D. Iwan, K.J. Stahl, The response of an elastic disk with a moving mass system, *Journal of Applied Mechanics* 40 (1973) 445–451.